Ceramics International 47 (2021) 16483–16490

Contents lists available at ScienceDirect

Ceramics International

journal homepage: www.elsevier.com/locate/ceramint

Sintering behaviour of fluorapatite–silicate composites produced from natural fluorapatite and quartz

D. Kherifi [a,b], H. Belhouchet [b], S. Ramesh [c,d,*], K.Y. Sara Lee [e], A. Kenzour [f,g], S. Djoualah [f], M.K. G. Abbas [c], Y.H. Wong [c], S. Ramesh [h]

[a] Physics and Chemistry of Materials Lab, Department of Physics, University Mohamed Boudiaf of M'sila, Algeria
[b] Physics Department, Faculty of Sciences, University Mohamed Boudiaf of M'sila, 28000, M'sila, Algeria
[c] Center of Advanced Manufacturing and Material Processing, Department of Mechanical Engineering, Faculty of Engineering, University of Malaya, 50603, Kuala Lumpur, Malaysia
[d] Department of Mechanical Engineering, Faculty of Engineering, Universiti Teknologi Brunei, Tungku Highway, BE1410, Brunei Darussalam
[e] Department of Mechanical Engineering, Faculty of Engineering and Technology, Tunku Abdul Rahman University College, Jalan Genting Kelang, 53300, Kuala Lumpur, Malaysia
[f] Optics and Precision Mechanics Institute, University of Ferhat, Abbas Setif 1, 19000, Setif, Algeria
[g] Research Center in Industrial Technologies CRTI, P.O. Box 64, 16014, Cheraga, Algiers, Algeria
[h] Centre for Ionics University of Malaya, Department of Physics, Faculty of Science, University of Malaya, 50603, Kuala Lumpur, Malaysia

ARTICLE INFO

Keywords:
Fluorapatite
Quartz
Composites
Sintering behaviour

ABSTRACT

In this work, the sintering behaviour of fluorapatite (FAp)–silicate composites prepared by mixing variable amounts of natural quartz (2.5 wt% to 20 wt%) and FAp was studied. The composites were pressureless sintered in air at temperatures from 1000 °C to 1350 °C. The effects of temperatures on the densification, phase formation, chemical bonding and Vickers hardness of the composites were evaluated. All the samples exhibited mixed phase, comprising FAp and francolite as the major constituents along with some minor phases of cristobalite, wollastonite, dicalcium silicate and/or whitlockite dependent on the quartz content and sintering temperature. The composite containing 2.5 wt% quartz exhibited the best sintering properties. The highest bulk density of 3 g/cm^3 and a Vickers hardness of >4.2 GPa were obtained for the 2.5 wt% quartz–FAp composite when sintered at 1100 °C. The addition of quartz was found to alter the microstructure of the composites, where it exhibited a rod-like morphology when sintered at 1000 °C and a regular rounded grain structure when sintered at 1350 °C. A wetted grain surface was observed for composites containing high quartz content and was believed to be associated with a transient liquid phase sintering.

1. Introduction

Calcium phosphate bioceramics, such as hydroxyapatite (HAp), carbonated HAp, fluorapatite (FAp) and chlorapatite (ClAp) are remarkably used for orthopaedics and orthodontic applications owing to their excellent biocompatibility, osseointegration and osteoconductive properties [1–9]. In particular, FAp ($Ca_{10}(PO_4)_6F_2$) has recently attracted considerable attention because the presence of fluoride enhances the biodegradability and compressive strength and stimulates the formation of bone tissues. Bogdanov et al. [10] demonstrated the viability of preparing fluorapatite glass ceramics by heat treatment process (i.e. melting at 1450 °C/2 h followed by crystallization at 680 °C/12 h) of glass mixture (SiO_2–Al_2O_3–P_2O_5–CaO–CaF). The XRD analysis revealed that FAp was the major crystalline phase with occasionally some minor phases such as apatite, norbergite, vitlokite, fluorphlogopite, fluormargarite and sellaite being present. Mirjalili et al. [11] investigated fluorapatite-based nanocomposites with additions of forsterite (up to 35%) and found that the bioactivity of the composites was enhanced and that the release of silicon ion when exposed in SBF solution intensified for samples containing forsterite. A similar improvement trend was also noted for the compressive strength of the FAp composites. However, a major issue with FAp is the low fracture toughness and poor wear-resistance exhibited by the sintered body, thereby limiting its application in the biomedical field [11]. Hence, different FAp-based

* Corresponding author. Center of Advanced Manufacturing and Material Processing, Department of Mechanical Engineering, Faculty of Engineering, University of Malaya, 50603, Kuala Lumpur, Malaysia.
E-mail address: ramesh79@um.edu.my (S. Ramesh).

https://doi.org/10.1016/j.ceramint.2021.02.216
Received 24 January 2021; Received in revised form 17 February 2021; Accepted 23 February 2021
Available online 25 February 2021

Table 1
Chemical composition (wt%) of natural FAp and natural quartz used in the present work.

Elements	F	Na_2O	MgO	Al_2O_3	SiO_2	P_2O_5	SO_3	K_2O	CaO	Fe_2O_3	ZnO	SrO	Y_2O_3	L.O.I.
FAp	3.65	1.13	0.89	0.87	1.79	28.2	2.55	0.138	59.9	0.455	0.038	0.345	0.044	–
Q	–	0.85	0.75	0.027	99.9	0.001	–	0.002	0.001	0.005	–	–	–	0.01

biocomposites, such as tricalcium phosphate- FAp (β-TCP-FAp) [12], kaolin- FAp [13], zinc oxide- FAp [14] and zirconia-FAp [15], have been studied to improve their mechanical properties.

Numerous studies have demonstrated that silica-containing bioceramics have excellent bioactivity and enhanced mechanical properties, thereby leading to the discovery of their potential in biomedical applications [16–18]. Fuh et al. [16] prepared micro-porous Si-substituted HAp by immersing hydroxyapatite compact disc in tetraethoxysilane (TEOS) followed by hydrolysis and condensation reaction to allow silicon gel formation before sintering. The authors found that the TEOS-treated HA possessed higher biaxial flexural strength and excellent cytocompatibility when compared to pure HAp having the same porosity level. Lin et al. [17] studied the effect of strontium (Sr) and silicon (Si) in $Sr_5(PO_4)_2SiO_4$ bioceramics on the *in vitro* cytocompatibility and osteogenic property for inducing osteanagenesis. Their results indicated that the simultaneous release of Sr and Si ions from the bioceramics played a significant role in improving the proliferation and osteogenic differentiation when compared with pure β-TCP. Khan et al. [18] affirmed the benefits of Si-substituted bioceramics and agreed that Si inclusion improved the biological performance of calcium phosphate based bioceramics. However, the authors inferred that the actual mechanism by which Si improves the osteoconductivity of the bioceramics remains unclear and requires further investigation.

In another study, the incorporation of a 50% wollastonite ($CaSiO_3$) phase in the HAp matrix successfully improved the compressive strength of sintered body by more than 50%, accompanied by higher degradation rate and excellent bioactivity compared with conventional HAp scaffold [19]. Sprio et al. [20] demonstrated that 20 wt% of dicalcium silicate (Ca_2SiO_4) is effective in aiding the densification of HAp. They found that the composite achieved 95% of theoretical density and flexural strength of 70.4 MPa when subjected to hot pressing at 1500 °C, whereas the flexural strength of monolithic HAp only attained 45 MPa [20]. In a recent study, kaolin-FAp composite was prepared, where the main compositions in kaolin are silica and alumina. The density and hardness of the composite increased with an increase in kaolin content. It was shown that the sample with the addition of 57 wt% kaolin achieved a relative density of 97% and the highest hardness of approximately 6.5 GPa when sintered at 1325 °C [13].

Borkowski et al. [21] studied the physicochemical and biological properties of FAp synthesised by using the sol-gel method and sintered at various temperatures. It was found that FAp sintered at 800 °C exhibited optimal porosity and fluoride release capacity thus enhancing the proliferation of osteogenic cells as compared to the control group. Golafshan et al. [22] prepared strontium-fluorapatite (Sr-FAp), magnesium and silicon-doped fluorapatite (Mg-SiFAp) by mechanochemical method. They found that the dopants were effective in promoting *in vitro* cellular proliferation and enhanced bone formation when compared to the undoped FAp. Other dopants such as alumina (Al_2O_3) was also found to be effective in promoting the sintering of FAp. Djoudallah et al. [23] investigated the reaction-sintering between fluorapatite and Al_2O_3 using natural phosphate and boehmite by mechanical mixing process. The sintering was performed in air atmosphere at various temperatures (1000–1500 °C). The results revealed that the densification and micro-hardness of FAp improved with increasing Al_2O_3 content and sintering temperature. It was found that the 25% Al_2O_3-doped FAp exhibited the highest density (2.95 g/cm^3) and hardness (6.5 ± 0.25 GPa) when sintered at 1450 °C. The authors also noted that the physical and mechanical properties of the FAp were influenced by the phases formed which were dependent on the alumina content and sintering conditions. Similar improvements in the mechanical properties were also reported by Youness et al. [24] for alumina-based carbonated fluorapatite.

In the present work, silicate-doped FAp composites were prepared for the first time by mixing natural FAp and quartz. This work aimed to investigate the effects of quartz addition up to 20 wt% on the phases and densification behaviour of FAp when subjected to pressureless sintering.

2. Materials and methods

The starting materials used in the present work are natural FAp and natural quartz (Q), which were obtained from Algeria [13]. Varying amounts of quartz, such as 2.5, 5, 10 and 20 wt% were mixed with FAp, and the samples were subsequently labelled as FA2.5Q, FA5Q, FA10Q and FA20Q, respectively. The mixing of the powder was accomplished by using a planetary ball mill (Fritsch P6) at a rotation speed of 350 rpm for 10 h. In a typical powder preparation, the required amounts of quartz and FAp powders were measured and placed inside a 250 ml zirconia jar containing zirconia balls (10 mm diameter) as the milling media and distilled water as the milling medium. The resulting mixture was dried at 120 °C for 24 h and sieved through a 100 μm mesh sieve after the milling is completed. The obtained powder was calcined at 900 °C for 2 h at a heating rate of 10 °C/min to remove any residual organic. The powders were then uniaxially pressed at 100 MPa to produce disc samples (13 mm diameter). The green samples were pressureless sintered in air at various temperatures between 1000 °C and 1350 °C for 2 h at a heating rate of 10 °C/min.

The phases present in the powders and sintered composites were identified through X-ray diffraction (XRD, X'Pert Pro, EMPYREAN, PANalytical, Netherlands) with CuKα radiation at 40 kV and 30 mA. The scan was conducted at a speed of 4°/min and step scan of 0.026°, over the 2θ from 20° to 55°. The phase identification was accomplished by comparing the XRD signatures of the sample with the database provided by the Joint Committee on Powered Diffraction Standards (JCPDS). The elemental composition of the samples was obtained through X-ray fluorescence (XRF).

The resulting chemical functional groups in the samples were determined from the Fourier transform infrared spectroscopy (FTIR) spectra taken over the wavenumber range of 2000 cm^{-1} to 400 cm^{-1} by using a Shimadzu IRAffinity-1S spectrophotometer. For this purpose, 2 mg of powder was mixed with 98 mg of potassium bromide for the FTIR study. Differential thermal analysis (DTA) of the composites was conducted with a LABSYS evo DTA/DSC Setaram equipment. The bulk density of the sintered samples was measured using the Archimedes method. A Vickers microhardness testing machine (Zwick-Roell, ZHV, Germany) was used to measure the hardness of the sintered samples under an indentation load of 300 g and loading time of 10 s. Prior to the hardness test, the samples were polished with a 6 and 1 μ diamond paste. Five measurements were taken on each sample to determine the average hardness. The microstructure of the fractured surface was examined with a Zeiss Sigma field emission scanning electron microscope (FESEM).

3. Results and discussion

The chemical compositions of FAp and quartz as determined from the XRF are presented in Table 1. The FAp in its natural form is composed mainly of CaO (59.9%) and P_2O_5 (28.2%), whereas the quartz comprises predominantly 99.9% SiO_2 with high purity. The XRD

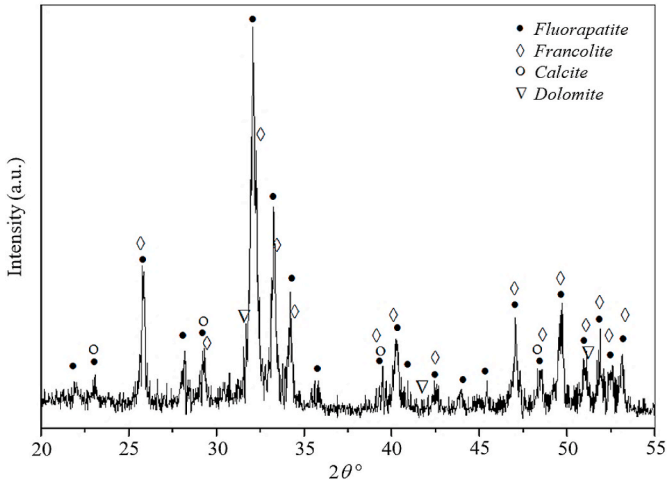

Fig. 1. XRD analysis of the as-received natural FAp powder showing a mix phase was present.

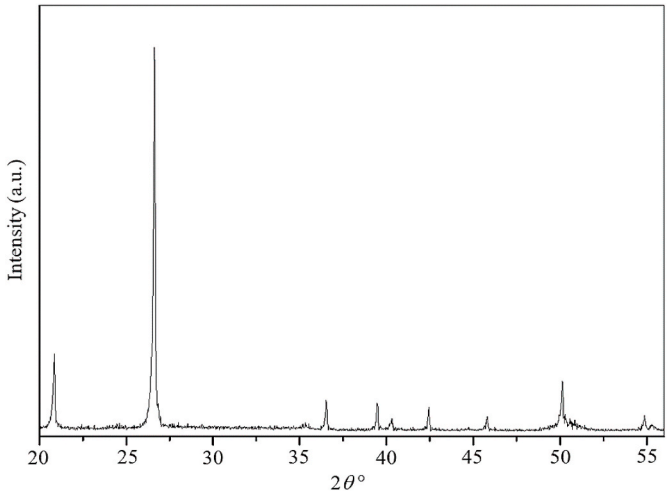

Fig. 2. XRD spectrum of the as-received natural quartz. All the peaks belongs to the SiO_2 phase.

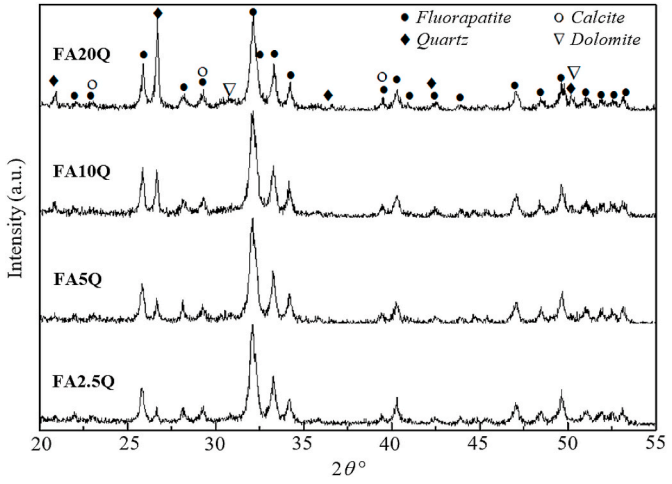

Fig. 3. Comparison of XRD signatures of the composite powders before calcination.

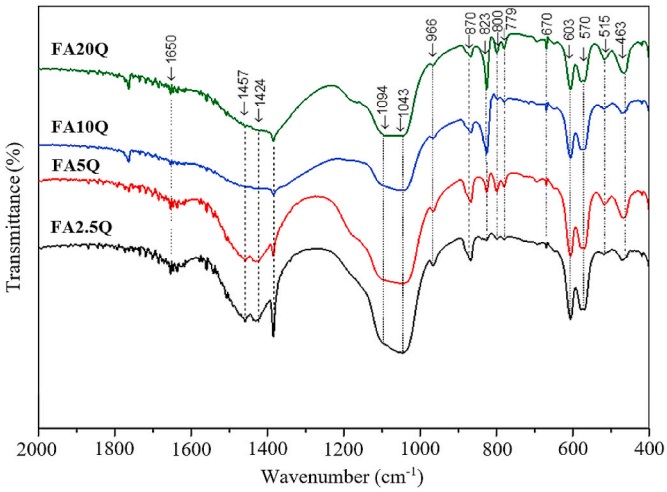

Fig. 4. FTIR spectra of composites before calcination.

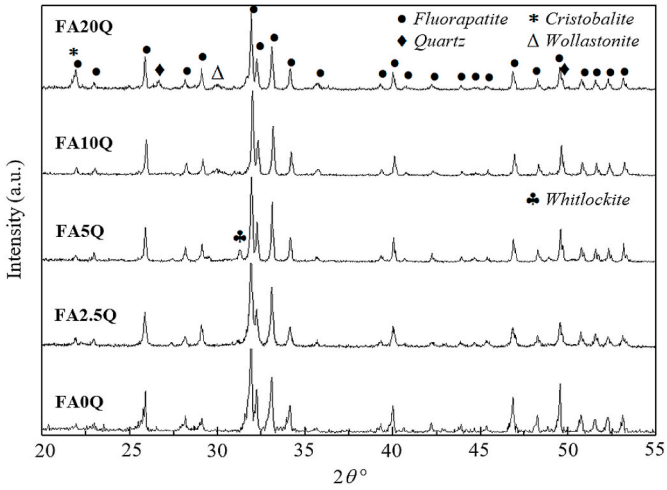

Fig. 5. XRD patterns of composite powders after calcination at 900 °C.

spectrum of the starting FAp (Fig. 1) showed that fluorapatite (JCPDS No. 15-876) and francolite (JCPDS No. 31-267) are the major phases, whereas dolomite (JCPDS No. 83-1530) and calcite (JCPDS No. 47-1743) represent the minor phases. For the natural quartz, silica (JCPDS No. 46-1045) was identified as the main phase (Fig. 2). The XRD patterns of the composite powders before calcination are shown in Fig. 3. Regardless of the quartz content, all mixtures exhibited the major crystalline phases of FAp and quartz, with small amounts of calcite and dolomite. The intensity of quartz, which is noticeable at $2\theta = 26.5°$, increases with the increased in quartz content in the mixture powder.

The FTIR spectra of the composite powders before calcination are presented in Fig. 4. The strong bands detected at 870 and 1385 cm^{-1} and the weak bands at 1424 and 1457 cm^{-1} are related to the presence of CO_3^{2-} group [25,26]. With the increase in the quartz content in FAp, the intensity of these bands decreases. Another strong band at 966 cm^{-1} is related to the mode ν_1 of PO_4^{3-} group, and the band at 1094 and 1043 cm^{-1} corresponds to the mode ν_3 of PO_4^{3-} group [26,27]. Two distinctive bands at 603 and 570 cm^{-1} are associated with the ν_4 of PO_4^{3-} group [26]. The intensity of the bands related to PO_4^{3-} group does not change with the addition of quartz. The bands at 823, 800, 779, 670, 515 and 463 cm^{-1} are associated with the silicate Si–O–Si network vibrations [25,28,29]. As expected, the intensity at 823 cm^{-1} strengthens with the increase in quartz content [30–32].

The effects of calcination on the phases present in the composite

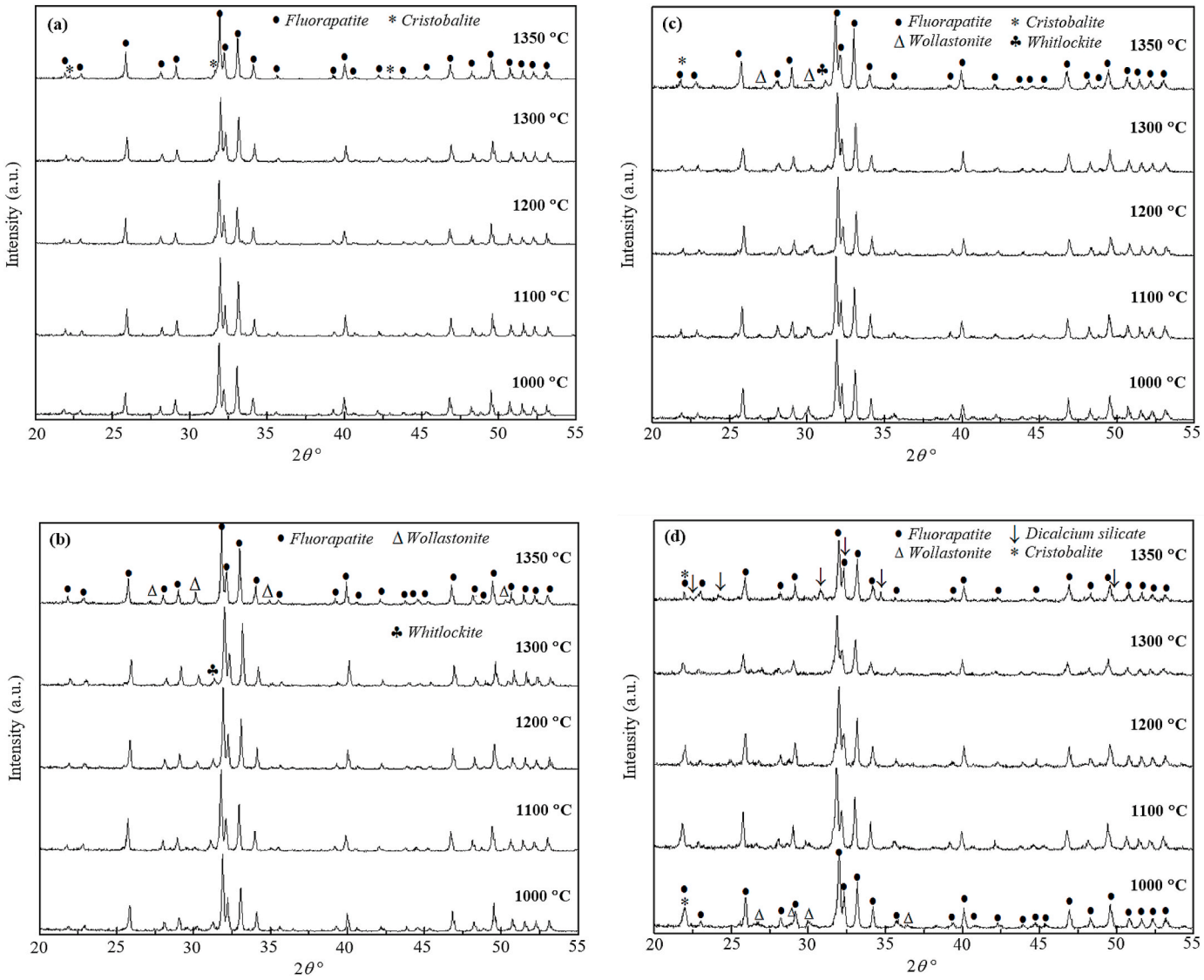

Fig. 6. XRD patterns for the various fluorapatite composites sintered at various temperatures: (a) FA2.5Q, (b) FA5Q, (c) FA10Q and (d) FA20Q.

powders are shown in Fig. 5. All composites consist of the major crystalline phases of FAp regardless of the quartz addition. The peak corresponding to that of quartz, particularly at 2θ ~26.5°, is clearly visible for the FA20Q sample when compared with the undoped powder (FA0Q). The phases that appeared in the composites after calcination include cristobalite (JCPDS No. 39-1425), wollastonite (JCPDS No. 43-1460) and whitlockite (JCPDS No. 09-0169). A strong peak of cristobalite is evident for the composite with 20 wt% quartz addition. Quartz start to transform into cristobalite at approximately 1190 °C and above [33]. However, in this work, the transformation from quartz to cristobalite occurred at a low temperature of 900 °C. A reaction between the FAp and excess quartz contributed to the reduction in quartz–cristobalite transformation temperature. The wollastonite peak started to appear when the composition of quartz was increased to 10 wt%. Free calcium oxide (CaO) decomposed from calcite ($CaCO_3$) and dolomite $CaMg(CO_3)_2$ due to the calcination at 900 °C [34]. The formation of wollastonite ($CaSiO_3$) as observed for FA10Q and FA20Q samples was due to the reaction between the free CaO and cristobalite (SiO_2) based on reaction [13] in accordance with Eq. (1).

$$CaO + SiO_2 \rightarrow CaSiO_3 \quad (1)$$

The formation of wollastonite was also due to the reaction between the calcite and excess SiO_2 present in the composites (FA10Q and FA20Q) in accordance with Eq. (2).

$$CaCO_3 + SiO_2 \rightarrow CaSiO_3 + CO_2 \quad (2)$$

In this work, the presence of whitlockite (tricalcium phosphate) in FA5Q can be associated with the decomposition of FAp at the calcination temperature to form tricalcium phosphate and CaF_2 [35] in accordance with Eq. (3).

$$Ca_{10}(PO_4)_6F_2 \rightarrow 3Ca_3(PO_4)_2 + CaF_2 \quad (3)$$

The XRD patterns of the composites containing different amounts of quartz and sintered at varying temperatures are shown in Fig. 6(a–d). The presence of FAp is clearly visible in all the composites regardless of the sintering temperatures and quartz content. The intensity of FAp is low in FA20Q (Fig. 6d) when sintered at 1300 °C and 1350 °C. This condition can be due to the partial fusion of FAp with quartz. For samples containing 5 wt% quartz and above, trace of whitlockite was detected at 2θ ~31.5° when sintered from 1000 °C to 1300 °C. However, this phase diminished when sintered at 1350 °C. The whitlockite was not detected in sample FA20Q throughout the sintering regime. A distinctive peak of wollastonite at 2θ ~30° was observed for sample FA5Q when sintered from 1200 °C to 1350 °C. The presence of wollastonite was

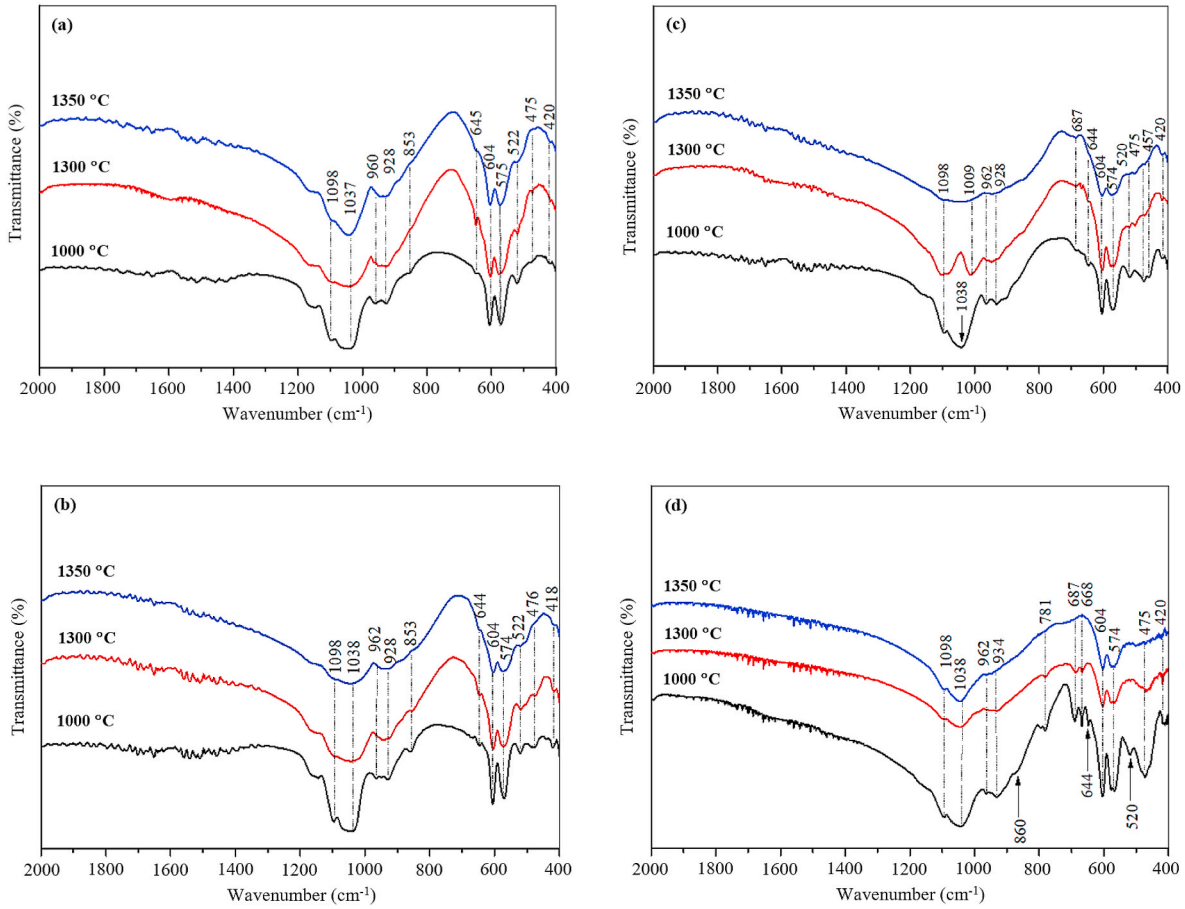

Fig. 7. FTIR analysis of composites sintered at various temperatures (a) FA2.5Q, (b) FA5Q, (c) FA10Q and (d) FA20Q.

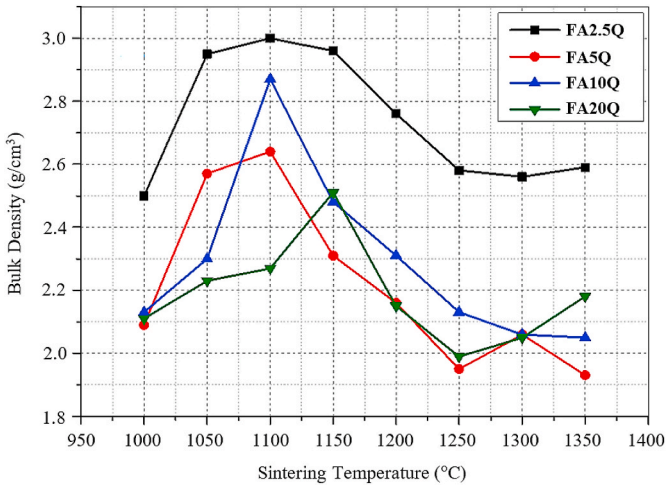

Fig. 8. Effect of sintering temperatures on the bulk density of fluorapatite composites.

Table 2
The bulk density and Vickers hardness of composites sintered at 1100 °C.

Sample	FA2.5Q	FA5Q	FA10Q	FA20Q
Bulk density (g/cm^3)	3.0 ± 0.10	2.63 ± 0.15	2.88 ± 0.17	2.28 ± 0.12
Vickers Hardness (GPa)	4.33 ± 0.32	4.67 ± 0.41	4.45 ± 0.36	4.42 ± 0.45

noticed for sample FA10Q at all sintering temperatures. The intensity of wollastonite peaks started to decrease in sample FA20Q when sintered from 1000 °C to 1100 °C, and this phase was not detected when sintered at 1200 °C and above. A strong peak of cristobalite at $2\theta \sim 22°$ was detected when the quartz content was increased to 20 wt%. The intensity of the cristobalite peak decreases when the sintering temperature increases from 1000 °C to 1350 °C. The formation of dicalcium silicate (JCPDS No. 20-0237) in this composite can be associated with the reaction between wollastonite ($CaSiO_3$) and CaO when sintered at high temperatures above 1200 °C on the basis of the reaction given in Eq. (4) [36].

$$CaSiO_3 + CaO \rightarrow Ca_2SiO_4 \quad (4)$$

The FTIR spectra for the composites sintered at 1000 °C, 1300 °C and 1350 °C are shown in Fig. 7(a–d). Regardless of quartz content, the absorption bands at 1098 and 1038 cm^{-1} corresponding to the v_3 antisymmetric vibration (stretching) mode of PO_4^{3-} group of FAp were present. Other bands corresponding to v_1 and v_4 vibration modes of PO_4^{3-} were observed at 962, 604 and 574 cm^{-1} [31]. However, the characteristic bands of carbonate at 870, 1424 and 1457 cm^{-1} (initially observed in Fig. 4) disappeared after sintering up to 1350 °C. The bands detected between 430 and 600 cm^{-1}, with a sharp peak around 520 cm^{-1} are attributed to the bending vibrations generated by the Si–O–Si group [37]. The bands existing at around 930 and 475 cm^{-1} are associated with the symmetric stretching mode of SiO_4^{4-} group [38,39]. The appearance of these bands can be due to the formation of calcium silicate phases, such as wollastonite and dicalcium silicate, during sintering.

The variation in bulk density of samples with different quartz contents sintered at various temperatures is shown in Fig. 8. For samples

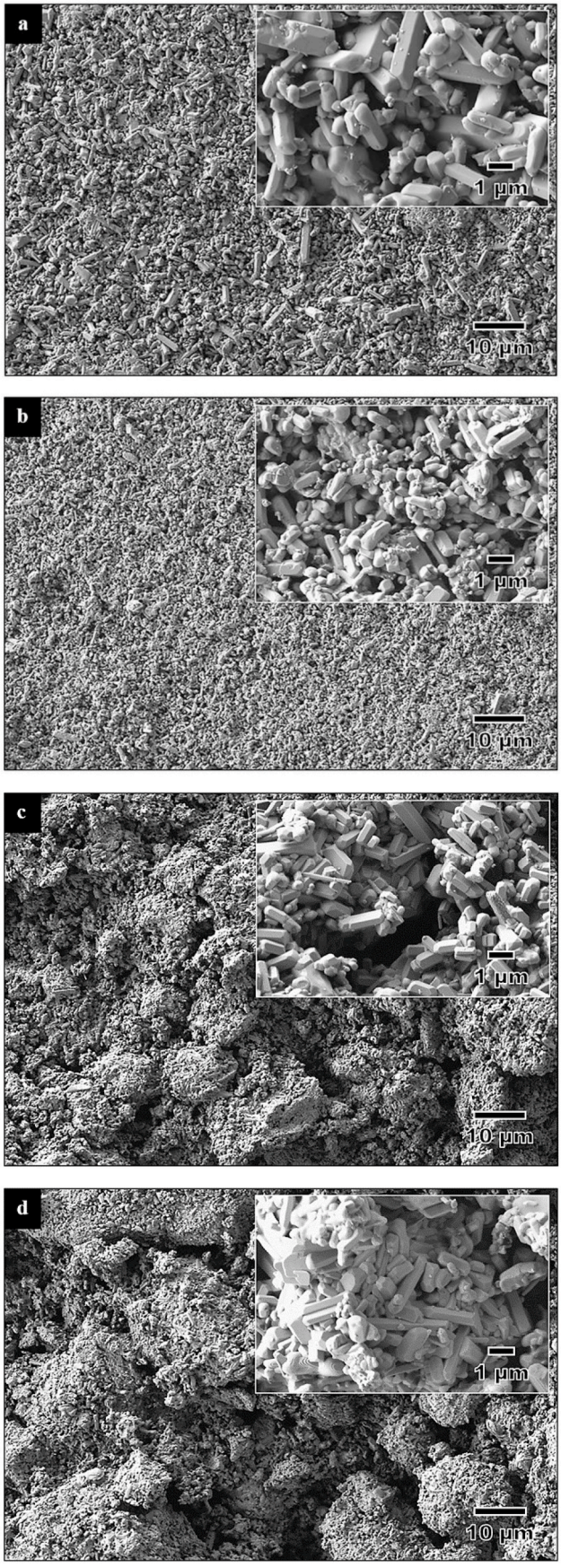

Fig. 9. SEM pictures of composites sintered at 1100 °C: (a) FA2.5Q, (b) FA5Q, (c) FA10Q and (d) FA20Q.

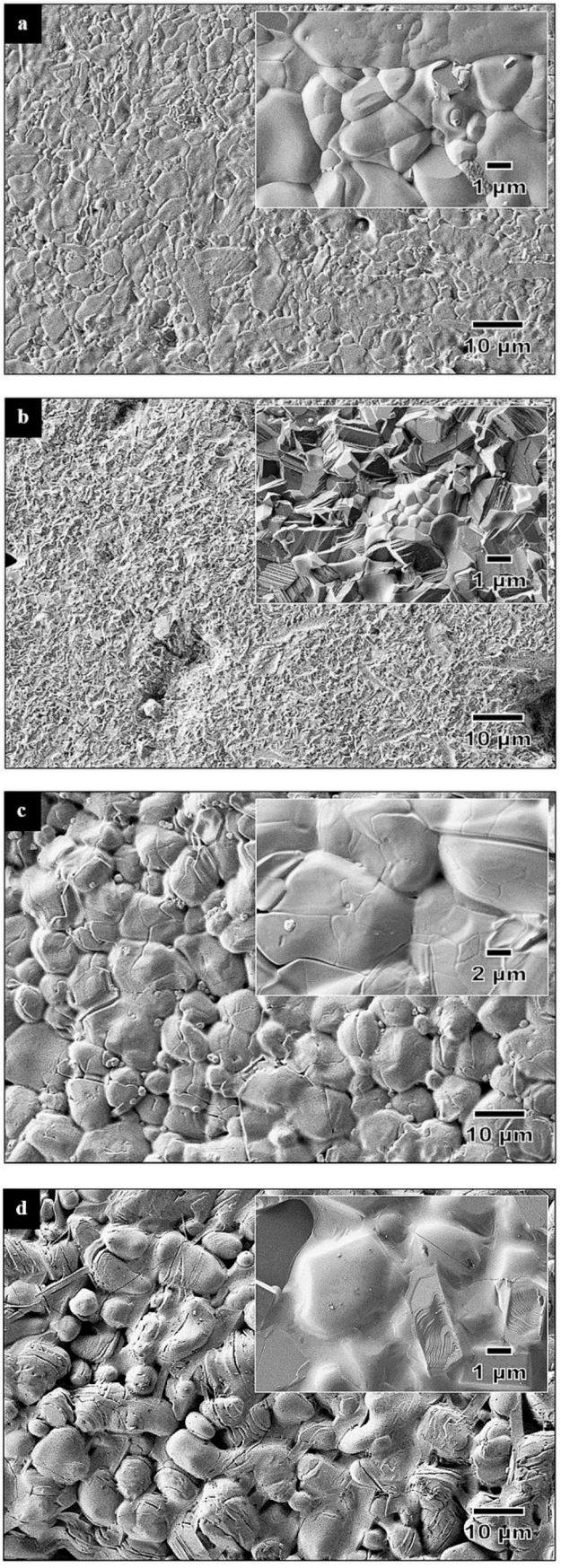

Fig. 10. Comparison of the SEM pictures of composites sintered at 1350 °C: (a) FA2.5Q, (b) FA5Q, (c) FA10Q and (d) FA20Q.

containing up to 10 wt% quartz, the density of the composites increased with the increase in sintering temperature, reached a maximum at approximately 1100 °C, and decreased with the increase in temperature. The composites with the lowest quartz content (FA2.5Q) exhibited the highest density among all the composites regardless of sintering temperature. The maximum density achieved was 3 ± 0.1 g/cm^3 when sintered at 1100 °C. The results suggested that the addition of 2.5 wt% quartz and when sintered from 1050 °C to 1150 °C are effective in enhancing the densification of FAp. Regardless of sintering temperatures, the addition of above 2.5 wt% quartz exhibited low densification. This condition can be attributed to the presence of secondary phases, such as whitlockite and wollastonite, as observed from the XRD analysis. In particular, the FA20Q samples exhibited the lowest densification with maximum bulk density of 2.5 ± 0.12 g/cm^3 measured for samples sintered at 1150 °C. For the Vickers hardness, measurement was only taken for the dense samples sintered at 1100 °C, as presented in Table 2. The hardness varied from 4.32 GPa to 4.67 GPa regardless of quartz addition, thereby indicating that no definite correlation was observed between the hardness and density of the composites.

The FESEM images of composites sintered at 1000 °C and 1350 °C are shown in Figs. 9 and 10, respectively. The morphology of composites evolved from rod-like structure to equiaxed grain morphology when the sintering temperatures increased from 1100 °C to 1350 °C. The composites with high quartz content (i.e. 10 wt% and 20 wt%) and when sintered at 1350 °C exhibited a wetted and smooth appearance of rounded grains. This condition is believed to be due to the excessive liquid phase that was present during sintering and rapidly cooled to room temperature (Fig. 10d). The SEM analysis of samples sintered at low temperature (Fig. 9) revealed a less dense structure, as clearly shown in the inset picture. This condition is in good agreement with the density measurement. However, as the sintering temperature was increased, this was accompanied by a denser microstructure, as shown in Fig. 10.

4. Conclusions

In this work, the effects of quartz addition and sintering temperature on the phase development and properties of natural FAp-sintered composites were investigated. The XRD analysis of the sintered composites indicated that a mix phase was obtained for all composites with FAp as the major phase regardless of sintering temperature. Minor phases of tricalcium phosphate were observed for composites containing 5 wt% and above quartz content. The formation of dicalcium silicate was observed for the sample with 20 wt% quartz addition and sintered at temperatures >1200 °C. This condition was found to have an adverse effect on densification due to the excessive wetting of transient liquid phase during sintering. These findings were supported by the FTIR analysis. This study showed that the addition of 2.5 wt% quartz is found to be effective in enhancing the densification and Vickers hardness of the FAp, particularly when sintered at low temperature of 1100 °C, which is beneficial for biomedical application.

Declaration of competing interest

The authors declare that they have no known competing financial interests or personal relationships that could have appeared to influence the work reported in this paper.

Acknowledgement

This research was supported under the FRGS grant no. FP020-2018A.

References

[1] K.S. Katti, Biomaterials in total joint replacement, Colloids Surf. B Biointerfaces 39 (2004) 133–142.
[2] N. Eliaz, N. Metoki, Calcium phosphate bioceramics: a review of their history, structure, properties, coating technologies and biomedical applications, Mater. (Basel, Switzerland) 10 (2017) 334.
[3] K. Tõnsuaadu, K.A. Gross, L. Plüduma, M. Veiderma, A review on the thermal stability of calcium apatites, J. Therm. Anal. Calorim. 110 (2012) 647–659.
[4] C.Y. Ooi, M. Hamdi, S. Ramesh, Properties of hydroxyapatite produced by annealing of bovine bone, Ceram. Int. 33 (2007) 1171–1177.
[5] G. Muralithran, S. Ramesh, The effects of sintering temperature on the properties of hydroxyapatite, Ceram. Int. 26 (2000) 221–230.
[6] I. Sopyan, M. Mel, S. Ramesh, K.A. Khalid, Porous hydroxyapatite for artifical bone applications, Sci. Technol. Adv. Mater. 8 (2007) 116–123.
[7] S. Ramesh, C.Y. Tan, S.B. Bhaduri, W.D. Teng, I. Sopyan, Densification behaviour of nanocrystalline hydroxyapatite bioceramics, J. Mater. Process. Technol. 206 (2008) 221–230.
[8] M. Safarzadeh, C.F. Chee, S. Ramesh, M.N. Ahmad Fauzi, Effect of sintering temperature on the morphology, crystallinity and mechanical properties of carbonated hydroxyapatite (CHA), Ceram. Int. 46 (2020) 26784–26789.
[9] M. Safarzadeh, S. Ramesh, C.Y. Tan, Hari Chandran, Y.C. Ching, A.F. Mohd Noor, S. Krishnasamy, W.D. Teng, Sintering behaviour of carbonated hydroxyapatite prepared at different carbonate and phosphate ratios, Bol. Soc. Espanola Ceram. Vidr. 59 (2020) 73–80.
[10] B.I. Bogdanov, P.S. Pashev, J.H. Hristov, I.G. Markovska, Bioactive fluorapatite-containing glass ceramics, Ceram. Int. 35 (2009) 1651–1655.
[11] F. Mirjalili, S. Manafi, F. Lotfi, Examination of morphology, degradation and biocompatibility of fluorapatite–forsterite nanocomposite, Ceram. Int. 46 (2020) 21256–21267.
[12] R. Taktak, A. Elghazel, J. Bouaziz, S. Charfi, H. Keskes, Tricalcium phosphate-fluorapatite as bone tissue engineering: evaluation of bioactivity and biocompatibility, Mater. Sci. Eng. C 86 (2018) 121–128.
[13] A. Kenzour, H. Belhouchet, M. Kolli, S. Djouallah, D. Kherifi, S. Ramesh, Sintering behavior of anorthite-based composite ceramics produced from natural phosphate and kaolin, Ceram. Int. 45 (2019) 20258–20265.
[14] B. Nasiri-Tabrizi, A. Fahami, Mechanochemical synthesis of fluorapatite-zinc oxide (FAp-ZnO) composite nanopowders, ISRN Ceram. (2012) 754704, 2012.
[15] B. Nasiri-Tabrizi, A. Fahami, Effect of zirconia content on the mechanosynthesis and structural features of fluorapatite-based composite nanopowders, Ceram. Int. 39 (2013) 7331–7342.
[16] L.J. Fuh, Y.J. Huang, W.C. Chen, D.J. Lin, Preparation of micro-porous bioceramic containing silicon-substituted hydroxyapatite and beta-tricalcium phosphate, Mater. Sci. Eng. C 75 (2017) 798–806.
[17] C. Lin, H. Zhu, Y. Zeng, Sr- and Si-containing bioceramic stimulate in vitro osteogenesis, Surf. Coating. Technol. 365 (2019) 129–133.
[18] A.F. Khan, M. Saleem, A. Afzal, A. Ali, A. Khan, A.R. Khan, Bioactive behavior of silicon substituted calcium phosphate based bioceramics for bone regeneration, Mater. Sci. Eng. C 35 (2014) 245–252.
[19] S.K. Padmanabhan, F. Gervaso, M. Carrozzo, F. Scalera, A. Sannino, A. Licciulli, Wollastonite/hydroxyapatite scaffolds with improved mechanical, bioactive and biodegradable properties for bone tissue engineering, Ceram. Int. 39 (2013) 619–627.
[20] S. Sprio, A. Tampieri, E. Landi, G.C. Celotti, D. Dalle Fabbriche, Bioactive hydroxyapatite/calcium silicate composites obtained by fast hot pressing: structure and flexural strength, Key Eng. Mater. 361–363 (2008) 423–426.
[21] L. Borkowski, A. Przekora, A. Belcarz, K. Palka, G. Jozefaciuk, T. Lübek, M. Jojczuk, A. Nogalski, G. Ginalska, Fluorapatite ceramics for bone tissue regeneration: synthesis, characterization and assessment of biomedical potential, Mater. Sci. Eng. C 116 (2020) 111211.
[22] N. Golafshan, M. Alehosseini, T. Ahmadi, A. Talebi, M. Fathi, M. Kharaziha, G. Orive, M. Castilho, A. Dolatshahi-Pirouzck, Combinatorial fluorapatite-based scaffolds substituted with strontium, magnesium and silicon ions for mending bone defects, Mater. Sci. Eng. C 120 (2021) 111611.
[23] S. Djouallah, H. Belhouchet, A. Kenzour, D. Kherifi, Sintering behavior of fluorapatite-based composites produced from natural phosphate and alumina, Ceram. Int. 47 (2021) 3553–3564.
[24] R.A. Youness, M.A. Taha, M. Ibrahim, Dense alumina-based carbonated fluorapatite nanobiocomposites for dental applications, Mater. Chem. Phys. 257 (2021) 123264.
[25] F.Z. Mezahi, A. Lucas Girot, H. Oudadesse, A. Harabi, Reactivity features of original sol-gel-derived 52S4 glass versus heat treatment temperature, J. Aust. Ceram. Soc. 54 (2018) 609–619.
[26] M. Azami, S. Jalilifiroozinezhad, M. Mozafari, M. Rabiee, Synthesis and solubility of calcium fluoride/hydroxy-fluorapatite nanocrystals for dental applications, Ceram. Int. 37 (2011) 2007–2014.
[27] A. Mokhtari, H. Belhouchet, A. Guermat, In situ high-temperature X-ray diffraction, FT-IR and thermal analysis studies of the reaction between natural hydroxyapatite and aluminum powder, J. Therm. Anal. Calorim. 136 (2019) 1515–1526.
[28] M. Montazerian, J.F. Schneider, B.E. Yekta, V.K. Marghussian, A.M. Rodrigues, E. D. Zanotto, Sol–gel synthesis, structure, sintering and properties of bioactive and inert nano-apatite–zirconia glass–ceramics, Ceram. Int. 41 (2015) 11024–11045.
[29] H. Belhouchet, F. Chouia, M. Hamidouche, A. Leriche, Preparation and characterization of anorthite and hydroxyapatite from Algerian kaolin and natural phosphate, J. Therm. Anal. Calorim. 126 (2016) 1045–1057.
[30] I. Denry, O.M. Goudouri, J. Harless, J.A. Holloway, Rapid vacuum sintering: a novel technique for fabricating fluorapatite ceramic scaffolds for bone tissue engineering, J. Biomed. Mater. Res. B Appl. Biomater. 106 (2018) 291–299.

[31] H.O. Amina Gharbi, A new glance at physico-chemical comportments of silicate bioactive glasses: influence of partial substitution: borosilicate versus fluorosilicate glasses, Int. J. Eng. Innov. Technol. 5 (2015) 74–80.
[32] I. Denry, J.A. Holloway, Low temperature sintering of fluorapatite glass-ceramics, Dent. Mater. 30 (2014) 112–121.
[33] L. Pagliari, M. Dapiaggi, A. Pavese, F. Francescon, A kinetic study of the quartz–cristobalite phase transition, J. Eur. Ceram. Soc. 33 (2013) 3403–3410.
[34] M. Olszak-Humienik, M. Jablonski, Thermal behavior of natural dolomite, J. Therm. Anal. Calorim. 119 (2015) 2239–2248.
[35] B. Nasiri-Tabrizi, A. Fahami, Reaction mechanisms of synthesis and decomposition of fluorapatite–zirconia composite nanopowders, Ceram. Int. 39 (2013) 5125–5136.
[36] N. Böhme, K. Hauke, M. Neuroth, T. Geisler, In situ Raman imaging of high-temperature solid-state reactions in the $CaSO_4$–SiO_2 system, Int. J. Coal Sci. Technol. 6 (2019) 247–259.
[37] N. Betancur-Granados, J.C. Restrepo, J.I. Tobón, O.J. Restrepo-Baena, Dicalcium silicate ($2CaO{\cdot}SiO_2$) synthesized through flame spray pyrolysis and solution combustion synthesis methods, Ceram. Int. 45 (2019) 9589–9595.
[38] P. Mazón, P.N. De Aza, Porous scaffold prepared from α′L-Dicalcium silicate doped with phosphorus for bone grafts, Ceram. Int. 44 (2018) 537–545.
[39] M.F. Zawrah, E.M.A. Hamzawy, Effect of cristobalite formation on sinterability, microstructure and properties of glass/ceramic composites, Ceram. Int. 28 (2002) 123–130.